JOURNAL OF GEOPHYSICAL RESEARCH, VOL. 116, D06304, doi:10.1029/2010JD014758, 2011

SO_2 emissions and lifetimes: Estimates from inverse modeling using in situ and global, space-based (SCIAMACHY and OMI) observations

Chulkyu Lee,[1,2] Randall V. Martin,[1,3] Aaron van Donkelaar,[1] Hanlim Lee,[4] Russell R. Dickerson,[5] Jennifer C. Hains,[6] Nickolay Krotkov,[7] Andreas Richter,[8] Konstantine Vinnikov,[5] and James J. Schwab[9]

Received 13 July 2010; revised 11 November 2010; accepted 29 November 2010; published 18 March 2011.

[1] Top-down constraints on global sulfur dioxide (SO_2) emissions are inferred through inverse modeling using SO_2 column observations from two satellite instruments (SCIAMACHY and OMI). We first evaluated the SO_2 column observations with surface SO_2 measurements by applying local scaling factors from a global chemical transport model (GEOS-Chem) to SO_2 columns retrieved from the satellite instruments. The resulting annual mean surface SO_2 mixing ratios for 2006 exhibit a significant spatial correlation ($r = 0.86$, slope = 0.91 for SCIAMACHY and $r = 0.80$, slope = 0.79 for OMI) with coincident in situ measurements from monitoring networks throughout the United States and Canada. We evaluate the GEOS-Chem simulation of the SO_2 lifetime with that inferred from in situ measurements to verify the applicability of GEOS-Chem for inversion of SO_2 columns to emissions. The seasonal mean SO_2 lifetime calculated with the GEOS-Chem model over the eastern United States is 13 h in summer and 48 h in winter, compared to lifetimes inferred from in situ measurements of 19 ± 7 h in summer and 58 ± 20 h in winter. We apply SO_2 columns from SCIAMACHY and OMI to derive a top-down anthropogenic SO_2 emission inventory over land by using the local GEOS-Chem relationship between SO_2 columns and emissions. There is little seasonal variation in the top-down emissions (<15%) over most major industrial regions providing some confidence in the method. Our global estimate for annual land surface anthropogenic SO_2 emissions (52.4 Tg S yr^{-1} from SCIAMACHY and 49.9 Tg S yr^{-1} from OMI) closely agrees with the bottom-up emissions (54.6 Tg S yr^{-1}) in the GEOS-Chem model and exhibits consistency in global distributions with the bottom-up emissions ($r = 0.78$ for SCIAMACHY, and $r = 0.77$ for OMI). However, there are significant regional differences.

Citation: Lee, C., R. V. Martin, A. van Donkelaar, H. Lee, R. R. Dickerson, J. C. Hains, N. Krotkov, A. Richter, K. Vinnikov, and J. J. Schwab (2011), SO_2 emissions and lifetimes: Estimates from inverse modeling using in situ and global, space-based (SCIAMACHY and OMI) observations, *J. Geophys. Res.*, *116*, D06304, doi:10.1029/2010JD014758.

1. Introduction

[2] Sulfur dioxide (SO_2) emissions from anthropogenic and natural sources are oxidized quickly in the atmosphere, leading to aerosol formation and acid deposition. Sulfate aerosols have highly uncertain effects on climate [*Intergovernmental Panel on Climate Change*, 2007; *U.S. Climate Change Science Program*, 2009], are deleterious to human health [*Katsouyanni et al.*, 1997], and degrade visibility [*Leaderer et al.*, 1979]. Assessments of the implications of SO_2 emissions usually are based on "bottom-up" inventories as estimated by using geographical and statistical data to extrapolate measurements of emission factors, typically available only on a sparse spatial and temporal network and subject to uncertainty. Moreover, bottom-up SO_2 emission inventories for a specific year quickly become outdated in a rapidly industrializing economy or through sulfur-reducing policy. Emissions moni-

[1]Department of Physics and Atmospheric Science, Dalhousie University, Halifax, Nova Scotia, Canada.
[2]National Institute of Meteorological Research, Korea Meteorological Administration, Seoul, South Korea.
[3]Harvard-Smithsonian Center for Astrophysics, Cambridge, Massachusetts, USA.
[4]Department of Atmospheric Science, Yonsei University, Seoul, South Korea.
[5]Department of Atmospheric and Oceanic Science, University of Maryland, College Park, Maryland, USA.
[6]Maryland Department of the Environment, Baltimore, Maryland, USA.
[7]Goddard Earth Sciences and Technology Center, University of Maryland, Baltimore County, Baltimore, Maryland, USA.
[8]Institute of Environmental Physics and Remote Sensing, University of Bremen, Bremen, Germany.
[9]Atmospheric Sciences Research Center, University at Albany, State University of New York, New York, USA.

toring is a fundamental component to a successful emissions reduction program [*Schakenbach et al.*, 2006]. "Top-down" constraints on SO_2 emissions through inverse modeling of satellite observations could provide valuable data to inform emission inventory development and evaluation.

[3] Inverse modeling has become a standard tool for combining observations of atmospheric composition with knowledge of atmospheric processes (transport, chemistry) to derive quantitative constraints on emissions to the atmosphere [e.g., *Müller and Stavrakou*, 2005; *Henze et al.*, 2007; *Kopacz et al.*, 2009]. It is implicitly assumed that the relationship between surface fluxes and atmospheric abundances is reasonably well predicted by the model, so that the biases between the model and the data are mostly due to errors in the emission inventories. Space-based observations of atmospheric traces gases have been used to provide top-down constraints on emissions including nitrogen oxides [e.g., *Leue et al.*, 2001; *Martin et al.*, 2003a; *Jaeglé et al.*, 2004; *Müller and Stavrakou*, 2005], CO [e.g., *Arellano et al.*, 2004; *Heald et al.*, 2004; *Pétron et al.*, 2004; *Kopacz et al.*, 2009], and VOCs [e.g., *Palmer et al.*, 2003; *Fu et al.*, 2007; *Millet et al.*, 2008]. To date, most top-down constraints on SO_2 emissions have focused on active volcanoes [e.g., *Carn et al.*, 2005]. Top-down constraints of anthropogenic SO_2 emissions are challenging in part due to the greater confidence in SO_2 emissions than other species [*Smith et al.*, 2010]. However, there is a growing interest in the application of satellite SO_2 data for insight into anthropogenic emissions [e.g., *Carn et al.*, 2007; *Georgoulias et al.*, 2009; *Li et al.*, 2010].

[4] An important consideration is the quality of SO_2 observations and their relationship with surface sources. SO_2 retrievals have developed markedly over the last decade using spectroscopic data available from a new generation of satellite spectrometers such as the Global Ozone Monitoring Experiment (GOME) [e.g., *Eisinger and Burrows*, 1998; *Khokhar et al.*, 2005; *Thomas et al.*, 2005], Scanning Imaging Absorption Spectrometer for Atmospheric Chartography (SCIAMACHY) [e.g., *Afe et al.*, 2004; *Richter et al.*, 2006; *Lee et al.*, 2008], Ozone Measurement Instrument (OMI) [e.g., *Krotkov et al.*, 2006, 2008; *Carn et al.*, 2007; *Yang et al.*, 2007], and Atmospheric Infrared Sounder (AIRS) [e.g., *Carn et al.*, 2005]. Satellite retrievals of SO_2 columns have been evaluated with in situ SO_2 profile measurements from aircraft [*Krotkov et al.*, 2008; *Lee et al.*, 2009] and column measurements from ground-based instruments [*Spinei et al.*, 2010]. Aircraft data offer precise in situ measurements, but these campaign-based comparisons are limited by sparse spatial and temporal sampling and by the need to extrapolate below the lowest measurement altitude. Ground-based measurements of SO_2 columns are sparse. In situ surface SO_2 measurements from dense networks when coupled with observed altitude profiles can offer an excellent opportunity to evaluate satellite retrievals.

[5] The removal mechanisms of atmospheric SO_2 dictate its impact on the environment. SO_2 removed by dry deposition has a local acidifying action, but SO_2 converted to sulfate has radiative and hydrological impacts. Measured deposition velocities for SO_2 [*Hicks*, 2006; *Myles et al.*, 2007] are generally 0.4 cm/s or slower giving a lifetime of about 3 days for a 1000 m deep planetary boundary layer. If the overall lifetime of SO_2 is much shorter than this, then the bulk of SO_2 is probably converted to sulfate with a longer lifetime and adverse impacts over a greater area. In situ measurements from the ground and aircraft offer a valuable data set to assess the SO_2 lifetime.

[6] We develop here top-down SO_2 emission estimates. Section 2 presents the SO_2 column retrieved from the satellite instruments (SCIAMACHY and OMI). Section 3 describes the atmospheric chemistry model (GEOS-Chem) used in this work and evaluates the GEOS-Chem simulation of the SO_2 lifetime. In section 4, we infer surface SO_2 mixing ratios from SCIAMACHY and OMI and evaluate the retrieved SO_2 columns with surface measurements. We estimate top-down SO_2 emissions and compare them with the bottom-up emissions in the GEOS-Chem model in section 5.

2. Satellite Retrieval of SO_2 Columns

2.1. Satellite Instruments (SCIAMACHY and OMI)

[7] The SCIAMACHY instrument, onboard ENVISAT, launched into a Sun-synchronous orbit in March 2002, provides the capability for solar observation of atmospheric SO_2 columns through observation of global backscatter [*Bovensmann et al.*, 1999]. SCIAMACHY observes the atmosphere in the nadir view with a typical surface spatial resolution of 30 km along track by 60 km across track, crossing the equator at 1000 local time (LT) in the descending node. Global coverage is achieved every 6 days.

[8] The OMI instrument onboard the Aura satellite is a nadir-viewing, imaging spectrometer that uses two-dimensional CCD detectors [*Levelt et al.*, 2006]. OMI measurements of the solar radiation backscattered by the Earth's atmosphere and surface can be applied to retrieve atmospheric SO_2 with a surface spatial resolution of up to 13 km by 24 km with global daily coverage. The Aura satellite was launched in July 2004 into a Sun-synchronous orbit with a local equator crossing time of 1330 LT in the ascending node.

2.2. SO_2 Retrieval From SCIAMACHY and OMI

[9] Satellite retrieval of total SO_2 columns from solar backscatter measurements used here involves three steps: (1) determining total SO_2 line-of-sight (slant) columns by spectral retrieval [*Richter et al.*, 2006; *Krotkov et al.*, 2006, 2008; *Lee et al.*, 2008], (2) removing the latitude-dependent offsets by using data from remote regions where the atmospheric contribution is small [*Lee et al.*, 2009], and (3) applying an air mass factor (AMF) to convert slant columns into vertical columns [*Lee et al.*, 2009].

[10] The SO_2 slant column retrieval for SCIAMACHY is based on the algorithms (Differential Optical Absorption Spectroscopy) of *Richter et al.* [2006] and *Lee et al.* [2008]. The wavelength range of 315–327 nm is used for the SO_2 fit which includes the SO_2 cross section (295 K) [*Vandaele et al.*, 1994], two ozone cross sections (223 K and 243 K) [*Bogumil et al.*, 2003], a synthetic Ring spectrum [*Vountas et al.*, 1998], an undersampling correction, and the polarization dependence of the SCIAMACHY instrument. Daily solar irradiance measurements taken with the ASM diffuser are used as the reference spectra. We use here the data taken at SZA $<70°$ and cloud radiance fraction <0.2.

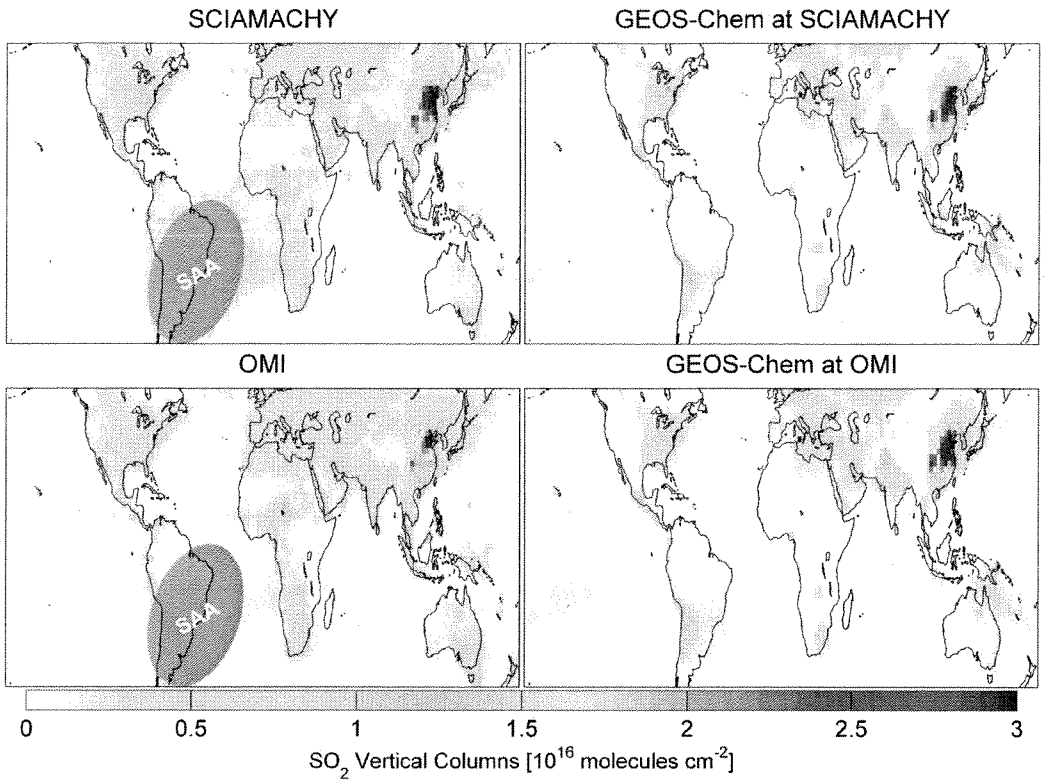

Figure 1. Annual mean SO_2 columns from SCIAMACHY, OMI, and GEOS-Chem for the year 2006 for cloud-radiance fraction <0.2. The right panels show GEOS-Chem SO_2 columns sampled coincidently with (top) SCIAMACHY and (bottom) OMI.

[11] For OMI we use the publicly released Planetary Boundary Layer (PBL) OMI SO_2 Level 2 product. The OMI SO_2 slant column data are retrieved with the Band Residual Difference algorithm [*Krotkov et al.*, 2006, 2008], based on the OMI TOMS-V8 algorithm [*Bhartia and Wellemeyer*, 2002]. SO_2 slant columns are inferred from corrected differential residuals at three wavelength pairs with large differential SO_2 cross sections in the OMI UV2 spectral region (P1 = 310.8–311.9; P2 = 311.9–313.2, and P3 = 313.2–314.4 nm) and differential SO_2 cross sections at 275 K [*Bogumil et al.*, 2003]. We use here the data with near-nadir viewing angles (cross track position from 20 to 40) at SZA <70° and cloud radiance fraction <0.2.

[12] *Lee et al.* [2009] removed the latitude-dependent offsets in SCIAMACHY and OMI SO_2 slant columns by subtracting the columns taken over the Pacific from the total column on a daily time scale. Then the slant columns were converted to vertical columns with the coincident local AMF. The AMF calculation combined a radiative transfer model (LIDORT) [*Spurr et al.*, 2001; *Spurr*, 2002] with spatially varying geophysical fields to account for atmospheric scattering and for absorption by O_3. The vertical distribution of SO_2 and aerosols for the local AMF calculation was locally determined with a global 3-D model of atmospheric chemistry GEOS-Chem (section 3.1). Here, we exclude SO_2 columns affected by eruptive volcanoes in SCIAMACHY and OMI measurements by excluding slant columns greater than 5 Dobson Units (1.34×10^{17} SO_2 molecules cm^{-2}), which we empirically determined. Annual mean SO_2 columns from SCIAMACHY and OMI for the year 2006 are shown in Figure 1. The largest values of more than 3×10^{16} molecules cm^{-2} are found over eastern China. Moderate enhancements of $1–2 \times 10^{16}$ molecules cm^{-2} exist over the eastern United States and South Africa.

[13] *Lee et al.* [2009] estimated the total error in the retrieval of SO_2 columns from SCIAMACHY and OMI. The retrieval error is dominated by the spectral fitting precision over remote regions. Over regions of enhanced SO_2 columns ($>1 \times 10^{16}$ molecules cm^{-2}) the AMF calculation becomes a more important contributor to the total error mostly due to uncertainty in clouds, SO_2 vertical profiles, surface reflectivity, and aerosols. The one-sigma SO_2 error from the AMF for individual, mostly clear (effective cloud fraction <0.2) observations over polluted regions is 20–40%, and likely contains a systematic component. *Lee et al.* [2009] evaluated the retrieved SO_2 columns with coincident airborne in situ measurements for campaigns over North America and the North Atlantic Ocean (r = 0.89, slope = 1.12 for SCIAMACHY and r = 0.92, slope = 0.95 for OMI) and east China (r = 0.9, slope = 1.0 for OMI).

3. Atmospheric Chemistry Model

3.1. GEOS-Chem

[14] The estimation of SO_2 emissions from satellite observation of SO_2 columns requires independent informa-

Table 1. Annual Global Sulfur Emissions in the GEOS-Chem Model for the year 2006

Source	Emission Rate, Tg S yr^{-1}
Fossil fuel on land	51.55
Ships[a]	4.72
Biomass burning	1.22
Biofuel burning	0.12
Aircraft	0.07
Volcano	6.55
Dimethyl sulfide (DMS)	21.05

[a]Emissions for ships are 1.7 Tg in coastal regions and 3.0 Tg in open ocean.

tion on the relationship of SO_2 columns to SO_2 emissions. A global 3-D model of tropospheric chemistry is the best source of this information considering the sparseness of in situ measurements and the large variability of SO_2 vertical profiles. We use the GEOS-Chem chemical transport model [*Bey et al.*, 2001] v8-01-04 (http://geos-chem.org) to obtain the SO_2 vertical distribution.

[15] GEOS-Chem is a global 3-D model of atmospheric composition driven by assimilated meteorological observations from the Goddard Earth Observing System (GEOS-4) at the NASA Goddard Global Modeling Assimilation Office (GMAO: http://gmao.gsfc.nasa.gov/). The GEOS-Chem model version used here has 30 vertical levels and a horizontal resolution of 2° latitude by 2.5° longitude. The aerosol simulation in GEOS-Chem includes the sulfate-nitrate-ammonium system [*Park et al.*, 2004], carbonaceous aerosols [*Park et al.*, 2003], sea salt [*Alexander et al.*, 2005], and mineral dust [*Fairlie et al.*, 2007]. The aerosol and oxidant simulations are coupled through formation of sulfate and nitrate [*Park et al.*, 2004], heterogeneous chemistry [*Jacob*, 2000; *Evans and Jacob*, 2005], and aerosol effects on photolysis rates [*Martin et al.*, 2003b; *Lee et al.*, 2009].

[16] Table 1 contains the global annual sulfur emissions used in the model. The global anthropogenic emission inventory for NOx, SOx, and CO is based on EDGAR [*Olivier et al.*, 2001] for the base year of 2000. The global inventory is replaced with regional inventories from NEI2005 (http://www.epa.gov/ttn/chief/net/2005inventory.html) over the United States for 2005, BRAVO [*Kuhns et al.*, 2005] over Mexico for 1999, CAC (http://www.ec.gc.ca/pdb/cac/cac_home_e.cfm) over Canada for 2005, Streets [*Zhang et al.*, 2009] for eastern Asia for 2006, and EMEP (http://www.emep.int) over Europe for 2005. All regional and global inventories are scaled from their respective base year to 2006 following *van Donkelaar et al.* [2008]. We replace the EDGAR ship emission inventory with the International Comprehensive Ocean-Atmosphere Data Set (ICOADS) [*Wang et al.*, 2008]. Natural sources of sulfur in the model include volcanoes and atmospheric oxidation of dimethyl sulfide (DMS) from phytoplankton. The oceanic water emission of DMS is calculated as the product of local seawater DMS concentration and sea-to-air transfer velocity [*Park et al.*, 2004]. Volcanic emissions of SO_2 from continuously active and sporadically erupting volcanoes are included from the database of *Andres and Kasgnoc* [1998] and the Global Volcanism Program (GVP: http://www.volcano.si.edu/) [*Lee et al.*, 2009].

[17] The GEOS-Chem sulfur simulation has been evaluated in a number of previous studies. GEOS-Chem generally gives unbiased simulation of sulfate aerosol concentrations over North America [*Park et al.*, 2004; *Heald et al.*, 2006]. The model can reproduce with no significant bias the observed vertical profiles of SO_x from aircraft campaigns of TRACE-P [*Park et al.*, 2004], INTEX-A [*Lee et al.*, 2009], and INTEX-B [*van Donkelaar et al.*, 2008; *Lee et al.*, 2009], although there is evidence that SO_2 oxidation may be too rapid over the North Pacific in spring [*Heald et al.*, 2006; *van Donkelaar et al.*, 2008].

[18] Figure 1 shows the annual mean of simulated SO_2 columns sampled coincidently (same day and time) with the SCIAMACHY and OMI observations. The coincident sampling used here reduces the effects of clouds and meteorology on the comparison of simulated and observed values. Noncoincident sampling would change the mean simulated values by <10% over most regions. Diurnal variation in the simulated SO_2 column from morning (SCIAMACHY) to afternoon (OMI) typically is <5%. The global distribution of the GEOS-Chem SO_2 columns is generally consistent with the observed columns from SCIAMACHY ($r = 0.79$, slope 1.59, offset = 1×10^{15} molecules cm^{-2}) and OMI ($r = 0.77$, slope = 0.89, offset = 2×10^{15} molecules cm^{-2}). However, there are notable differences over China.

3.2. Evaluation of SO_2 Lifetime in GEOS-Chem

[19] The SO_2 lifetime is a critical parameter in the inversion of SCIAMACHY and OMI SO_2 columns for SO_2 emissions. Here we evaluate the GEOS-Chem simulation of the SO_2 lifetime by comparison with that inferred from in situ measurements.

[20] *Hains* [2007] analyzed SO_2 vertical profiles measured from aircraft to calculate the in situ measurement-based lifetime. The aircraft campaigns [*Taubman et al.*, 2006; *Hains et al.*, 2008] were conducted from June to August 1995–2005 in the mid-Atlantic region (35.21°N – 44.51°N, 68.41°W–81.61°W). Over 50% of the spirals were made in Maryland, Virginia and Pennsylvania. All flights were made during daytime (midmorning or midafternoon) on days when smog events were forecast. Flights were made between small regional airports. Spirals made over the airports from the surface to roughly 3 km above sea level were completed within 30 min. The SO_2 instrument (TEI Model 43C) was zeroed at the bottom and top of each spiral. Flight patterns were generally chosen to capture transport of pollutants to locations downwind of urban locations, thus flights conducted in the morning (before noon EST) were typically upwind of urban areas in the mid-Atlantic, while flights conducted in the afternoon (after noon EST) were typically downwind of urban locations (mainly the Baltimore, Washington, and Philadelphia metropolitan areas).

[21] The measured SO_2 profiles show little difference between the morning and afternoon. Both profiles show greater values near the surface that decrease with altitude, possibly resulting from oxidation by H_2O_2 in fair weather cumulus (common under summertime high-pressure systems and often encountered during these flights) as SO_2 mixes vertically. Assuming that SO_2 in the lower troposphere is destroyed on time scales fast relative to advection from the region (and then the rate of emissions into the atmosphere is equal to the rate of loss in the atmosphere), the calculated lifetime is 19 ± 7 h on average (at the 95% confidence level) [*Hains*, 2007].

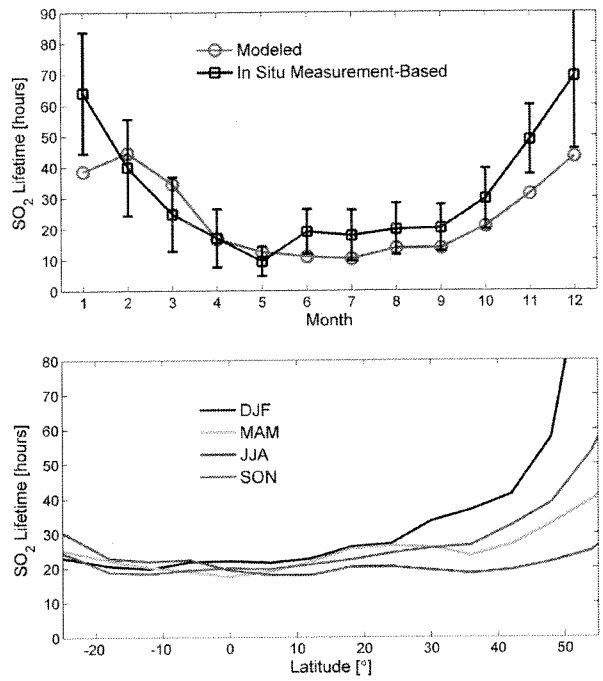

Figure 2. (top) Monthly SO_2 lifetime in the daytime mixed layer over the eastern United States (35.2°N–44.5°N, 68.4° W–81.6°W). The in situ measurement-based lifetime as calculated with equation (1) is indicated with black squares. Red circles indicate the lifetime from the GEOS-Chem simulation. Error bars are given by $\tau_{Mon} \times \sqrt{\left(\frac{\sigma_{JJA}}{\tau_{JJA}}\right)^2 + \left(\frac{\sigma_{Mon}}{C_{Mon}}\right)^2} \times \frac{1}{n}$, where τ_{Mon} is monthly mean lifetime of SO_2, σ_{JJA} is the standard deviation of 7 h of SO_2 summer lifetime (τ_{JJA} = 19 h) from *Hains* [2007], and σ_{Mon} is the standard deviation of mean daytime SO_2 mixing ratios (C_{Mon}) at in situ measurements sites over the eastern United States. (bottom) Seasonal zonal mean lifetime of SO_2 in the boundary layer from the GEOS-Chem model for December–February (DJF), March–May (MAM), June–August (JJA), and September–November (SON) for the year 2006.

[22] The mean SO_2 lifetime from our GEOS-Chem simulation over the mid-Atlantic region for daytime (0900–1700) of June–August 2006 is 13 h, within the range inferred by *Hains* [2007]. The shorter lifetime in the model is consistent with previous indications that GEOS-Chem SO_2 oxidation may be too rapid [*Heald et al.*, 2004; *van Donkelaar et al.*, 2008]. Sampling the model on days similar to the flight conditions (daily afternoon O_3 > mean June–August afternoon O_3) decreases the SO_2 lifetime in GEOS-Chem by <3 h.

[23] Of interest for our work is the seasonal variation of the SO_2 lifetime. For that purpose we use ground-based in situ measurements from the U.S. Environmental Protection Agency's Air Quality System (AQS). SO_2 emissions for the eastern United States vary by less than 20% throughout the year [*U.S. Environmental Protection Agency*, 2009]. Thus the monthly variation in the SO_2 lifetime is linearly proportional to the monthly SO_2 mixing ratio C_{Mon} after correcting for monthly variation in the boundary layer height H_{Mon}, and assuming no seasonal change in the rate of mixing between the boundary layer and the free troposphere. We extend the in situ measurement-based SO_2 lifetime τ_{JJA} of 19 h for July to August from *Hains* [2007] to the rest of the year 2006 by using observed surface SO_2 mixing ratios and boundary layer heights from the GEOS-4 assimilation. Assuming SO_2 emissions are seasonally invariant, the in situ measurement-based SO_2 lifetime τ_{Mon} can be given by

$$\tau_{Mon} = \tau_{JJA} \times \frac{C_{Mon}}{C_{JJA}} \times \frac{H_{JJA}}{H_{Mon}} \quad (1)$$

where subscript "Mon" and "JJA" denote month and mean for June to August, respectively. C is obtained from in situ surface SO_2 concentrations at 14 in situ measurement sites from the AQS network and a research site [*Schwab et al.*, 2009] within the mid-Atlantic region (35.21°N–44.51°N, 68.41°W–81.61°W), and H is taken from GEOS meteorological fields over the same area.

[24] The black lines in Figure 2, top, show that the resulting lifetime values range from 15 h in summer to 65 h in winter. The red lines show the daytime SO_2 lifetime over the same domain from the GEOS-Chem simulation as determined by gas-phase oxidation, dry deposition, and aqueous oxidation in clouds. The simulated and measurement-based lifetimes exhibit a high degree of consistency. The RMS difference is 2.2 h. The longer SO_2 lifetime in winter reflects reduced oxidation by both aqueous (i.e., H_2O_2) and gas-phase (i.e., OH) processes.

[25] Figure 2, bottom, shows the seasonal zonal mean lifetime of SO_2 calculated using the GEOS-Chem model during the daytime of 0900–1700 LT for the rest of the world. The lifetime is within the range of previous results for the global averages of 0.6 – 2.6 days [e.g., *Chin and Jacob*, 1996; *Restad et al.*, 1998; *Berglen et al.*, 2004]. The lifetime at northern midlatitudes where anthropogenic emissions dominate is 16–40 h exhibiting clear seasonal variation with a maximum in winter (DJF) and a minimum in summer (JJA). Values for spring (MAM) are similar to fall (SON). The 24 h SO_2 lifetime is within 10% of that shown here for daytime. *Chin et al.* [1996] explain the longer SO_2 lifetime in winter due to slower dry deposition velocities, and reduced supply of oxidants (H_2O_2 and OH) in winter. *Alexander et al.* [2009] used isotopic measurements to infer a significant role for transition metal-catalyzed oxidation of atmospheric SO_2; neglect of this mechanism here may contribute to an overestimate of the SO_2 lifetime at high latitudes in winter.

4. Evaluation of SCIAMACHY and OMI SO_2 With Surface Measurements

[26] Aircraft measurements reveal that SO_2 within the boundary layer typically makes a dominant contribution to SO_2 columns over land except in volcanic regions [*Taubman et al.*, 2006; *Hains et al.*, 2008; *Lee et al.*, 2009]. GEOS-Chem simulations of annual mean SO_2 columns and of surface SO_2 concentrations exhibit significant spatial correlations over land (r = 0.95, n = 13,104) and over North America (r = 0.97, n = 325). Thus we infer surface SO_2 mixing ratios from SCIAMACHY and OMI observations of

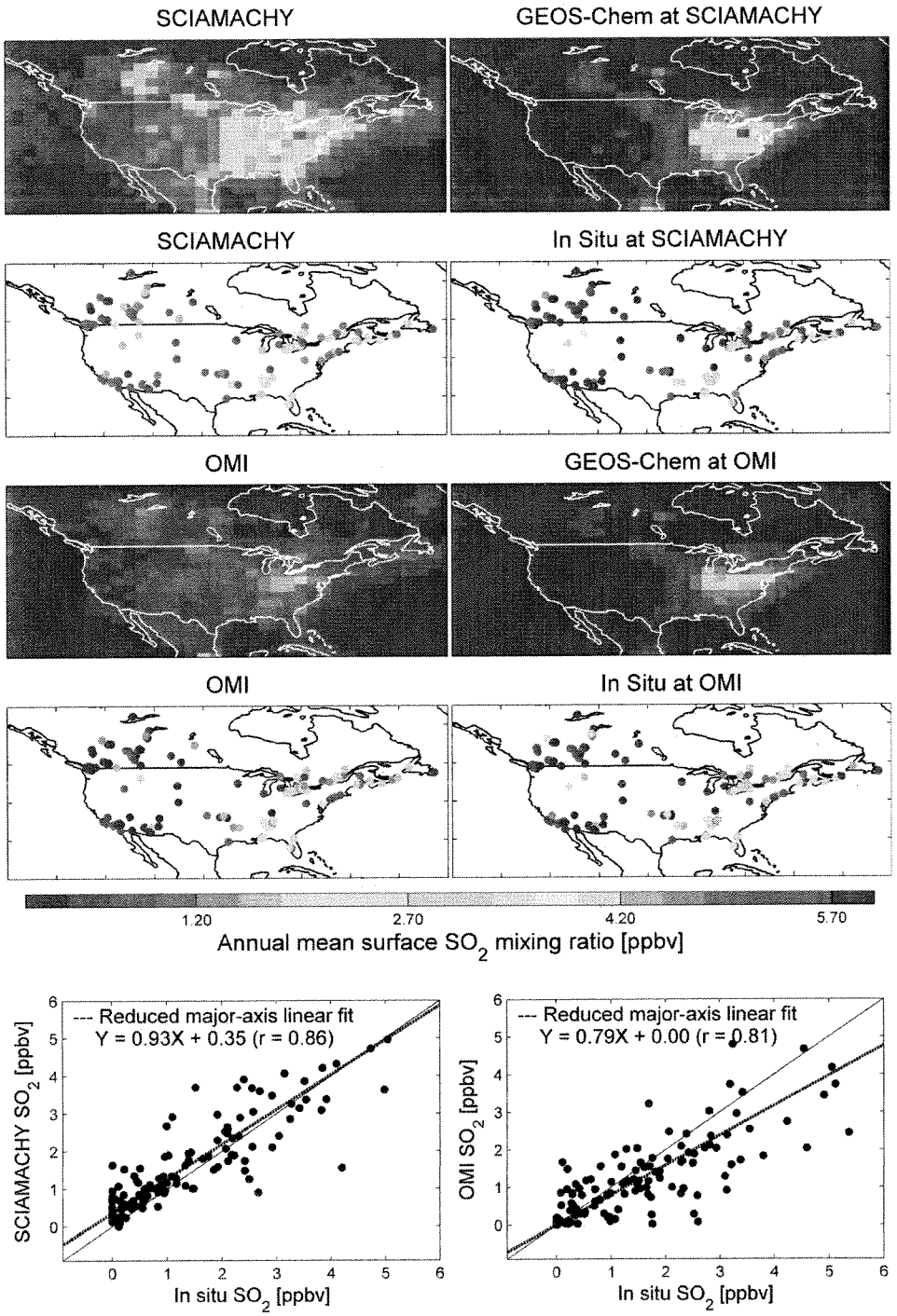

Figure 3. Annual mean of surface SO_2 mixing ratios for the year 2006. The left column contains surface SO_2 mixing ratios inferred from SCIAMACHY and OMI for cloud-radiance fraction <0.2. The right column contains coincident surface SO_2 mixing ratios from GEOS-Chem simulations and in situ measurements. The bottom row shows the scatterplots of annual mean surface SO_2 mixing ratios from SCIAMACHY and OMI versus those from the in situ measurements. In the scatterplots, the solid lines represent the Y = X line, and the dotted lines were calculated with reduced major-axis linear regression [*Hirsch and Gilroy*, 1984].

SO_2 columns for evaluation with ground-based in situ measurements over North America.

4.1. Ground-Based in Situ Measurement

[27] Hourly measurements of SO_2 are obtained from the U. S. Environmental Protection Agency (EPA)'s Air Quality System (AQS) and Environment Canada's National Air Pollution Surveillance (NAPS) network. We average the hourly in situ measurements over a 2 h period (0900–1100 LT for SCIAMACHY and 1300–1500 LT for OMI) to correspond with respective satellite observation times over North America.

4.2. Surface SO_2 Inferred From Satellite Observations

[28] We use the GEOS-Chem local SO_2 profile to estimate surface-level SO_2 mixing ratios from retrieved SO_2 columns. Similar applications have been conducted for aerosol [*Liu et al.*, 2004; *van Donkelaar et al.*, 2006, 2010] and NO_2 [*Lamsal et al.*, 2008]. Local SO_2 profiles coincident with the SCIAMACHY or OMI observations are taken from the GEOS-Chem simulation. A general equation to infer the surface SO_2 mixing ratio S_{Sat} from the satellite-measured SO_2 columns Ω_{Sat} is

$$S_{Sat} = \frac{S_{GC}}{\Omega_{GC}} \times \Omega_{Sat} \quad (2)$$

where subscript "GC" denotes GEOS-Chem. The satellite derived surface SO_2 represents the mixing ratio at the lowest vertical layer (100 m) of the model. Spatial variation in the satellite observations within 2° × 2.5° resolution of the GEOS-Chem simulation reflects spatial variation of SO_2 mixing ratios in the boundary layer.

[29] *Lamsal et al.* [2008] developed a scheme to infer surface NO_2 concentrations at the OMI measurement resolution, accounting for variation of the profiles within a GEOS-Chem grid. Here we apply it to infer surface SO_2 mixing ratios at the satellite measurement resolution. Assuming that the simulated free tropospheric SO_2 column Ω_G^F is horizontally invariant over a GEOS-Chem grid, reflecting the longer SO_2 lifetime in the free troposphere, the corresponding surface SO_2 mixing ratio S'_{Sat} is given by

$$S'_{Sat} = \frac{\nu \cdot S_{GC}}{\nu \cdot \Omega_{GC} - (\nu - 1)\Omega_{GC}^F} \times \Omega_{Sat} \quad (3)$$

where ν represents the ratio of the local satellite SO_2 column to the mean satellite field over the GEOS-Chem grid. Equation (3) equals equation (2) for a unity value of ν. SO_2 mixing ratios calculated with equation (3) differ from those calculated with equation (2) by up to ± 20% in polluted areas.

[30] Annual mean surface SO_2 mixing ratios inferred from SCIAMACHY and OMI over North America are shown in 1st and 3rd rows of Figure 3, regridded onto the GEOS-Chem grid of 2° by 2.5°. Both SCIAMACHY and OMI show enhanced SO_2 over industrial regions of the eastern United States, and are highly correlated (r = 0.89) with each other. However, the SCIAMACHY-derived SO_2 mixing ratios tend to be higher by 2.6 times (2.5 ppbv) than those from OMI over industrial regions of the eastern United States. Contributing factors include diurnal variation in mixed layer depth and chemistry, and errors in the SO_2 column retrievals. The GEOS mixed layer depth sampled at OMI overpass is typically 25–30% higher than at SCIAMACHY overpass. Simulated SO_2 sampled at SCIAMACHY overpasses over those regions is twice (1.5 ppbv) those at OMI overpasses, reflecting diurnal variation in both chemistry and mixed layer depth. Retrieval bias may contribute to the remaining differences between SCIAMACHY and OMI.

[31] The 2nd and 4th rows of Figure 3 show the annual mean surface SO_2 mixing ratios inferred from the ground-based in situ measurements at AQS/NAPS network sites throughout the United States and Canada. Satellite measurements with pixel centers within 15 km of the measurement sites are used for the comparison. We exclude sites with <20 coincident measurements over the year. SO_2 inferred from satellite observations is in relatively poor (r < 0.4) temporal agreement with in situ measurements for the year 2006, reflecting relatively high uncertainty in individual retrievals. However, Figure 3, bottom, indicates that the annual mean surface SO_2 mixing ratios from SCIAMACHY and OMI are spatially well correlated with coincident in situ measurements (r = 0.86, slope = 0.93, n = 115 for SCIAMACHY and r = 0.81, slope = 0.79, n = 121 for OMI). The better correlation and slope for SCIAMACHY than OMI could reflect the use of longer wavelengths in the SCIAMACHY retrieval that are more sensitive to SO_2 in the boundary layer. The mean bias (satellite/in situ) is 1.19 for SCIAMACHY and 0.79 for OMI. Simulated surface SO_2 mixing ratios also exhibit consistency (r = 0.83, slope = 0.84 for SCIAMACHY sampling and r = 0.83, slope = 0.81 for OMI sampling) with the in situ measurements. The less than unity slope in both the modeled and retrieved values could reflect unresolved subgrid variability.

[32] Although our objective here is application of surface SO_2 concentrations for evaluation of satellite observations, the satellite-derived surface SO_2 concentrations could be of value for long-term estimates of air pollution. The spatial distribution of GEOS-Chem simulations of annual mean surface SO_2 concentrations are well correlated with annual mean surface sulfate concentrations over North America (r = 0.90, n = 325) and over land globally (r = 0.86, n = 13104).

5. Seasonal Bottom-Up and Top-Down Emissions of SO_2

[33] We go on to infer top-down emissions from the satellite SO_2 columns through inverse modeling. We first evaluate the fraction of the SO_2 column from anthropogenic activity to guide the emission analysis. Then we describe the approach to estimate the top-down emissions from SCIAMACHY and OMI observations of SO_2 columns. The seasonal satellite-based top-down estimates are compared with the seasonal bottom-up emission inventories described in section 3.

5.1. Anthropogenic Fraction of SO_2 Column

[34] Figure 4, top, shows annual mean SO_2 columns simulated with GEOS-Chem for the year 2006. The standard emission inventory in the GEOS-Chem model including volcanoes and DMS is used here as the bottom-up inventory (section 3). Most SO_2 enhancements exist over and immediately downwind of industrial regions including the eastern United States, eastern China, and northern India.

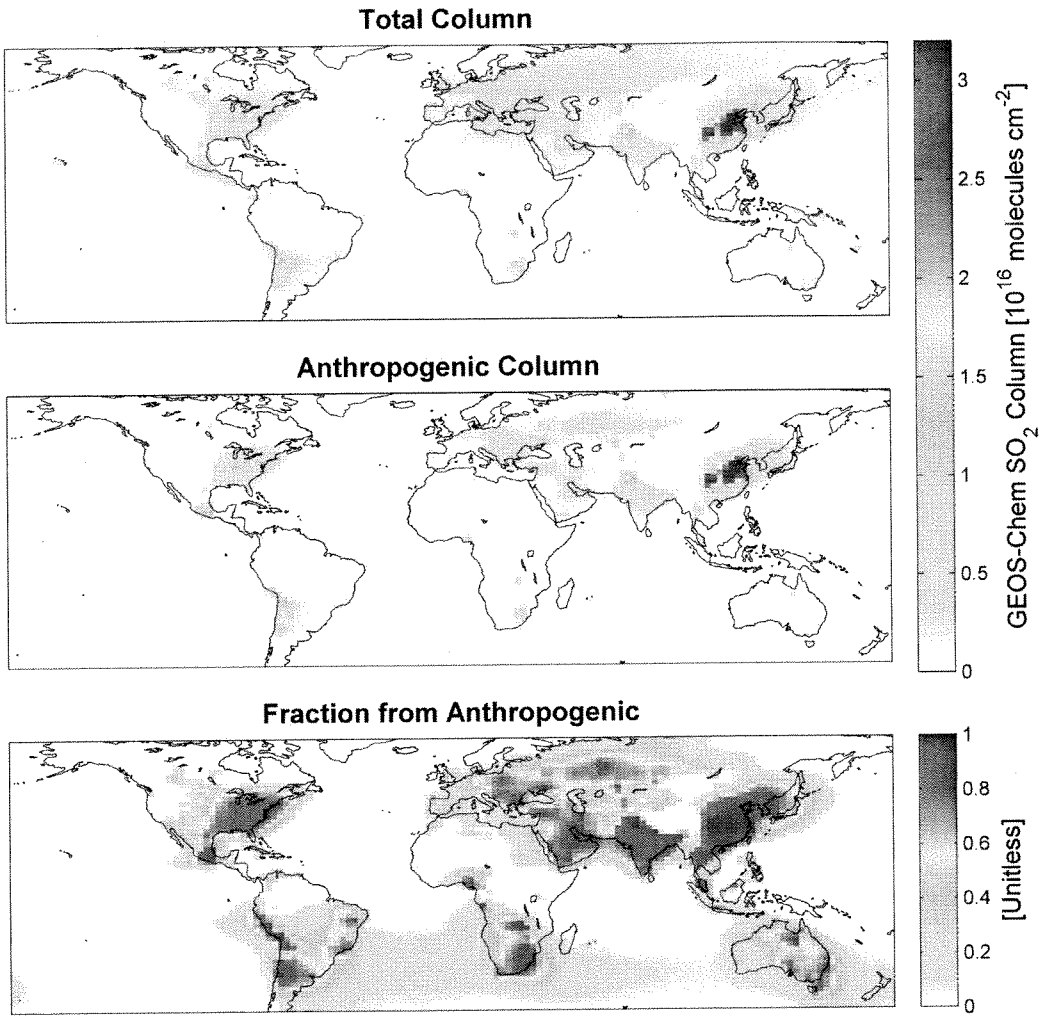

Figure 4. Annual mean SO_2 columns determined from the GEOS-Chem model for the year 2006 with (top) the standard SO_2 emissions inventories as described in section 2, and (middle) anthropogenic emission inventories only. (bottom) The fraction of SO_2 columns from the anthropogenic SO_2 emissions is calculated by dividing Figure 4, top, by Figure 4, middle.

Figure 4, middle, shows a sensitivity simulation with anthropogenic emissions only. The fraction of SO_2 columns from anthropogenic SO_2 emissions is shown Figure 4, bottom. Anthropogenic activities contribute >60% of total SO_2 columns over large regions of all continents. Exceptions are over regions with low SO_2 columns such as the Sahara and Amazon. The anthropogenic SO_2 fraction rarely exceeds 40% over the open ocean. We focus our anthropogenic emission analysis over land.

5.2. Top-Down Emissions From SCIAMACHY and OMI SO_2 Columns

[35] We infer a top-down SO_2 emission inventory E_T from satellite SO_2 columns Ω_{Sat} using the mass balance approach following *Martin et al.* [2003a],

$$E_T = \frac{E_B}{\Omega_{GC}} \times \Omega_{Sat} \quad (4)$$

where E_B is the bottom-up emission inventory described in section 3 and Ω_{GC} is the simulated SO_2 column. The ratio of E_B/Ω_{GC} is an effective, first-order, SO_2 rate constant that accounts for local SO_2 chemistry and transport. Ω_{GC} is sampled coincidently with Ω_{sat}. The smearing length scale [*Palmer et al.*, 2003] is of order 100 km comparable to the GEOS-Chem resolution used here. Therefore we neglect smearing in this initial analysis. Smearing is of most concern in winter when wind speeds are higher and the SO_2 lifetime is longer. Annual mean SO_2 columns simulated from the GEOS-Chem model exhibit significant spatial correlation with the bottom up SO_2 emissions over land ($r = 0.85$, $n = 13104$), over North America ($r = 0.88$, $n = 325$), and over eastern China ($r = 0.90$, $n = 154$).

[36] We apply this method to land surface and coastal ship emissions only. Inferring SO_2 from DMS oxidation and ship emissions over the open ocean would involve a more sophisticated inversion, such as an adjoint [e.g., *Henze et al.*,

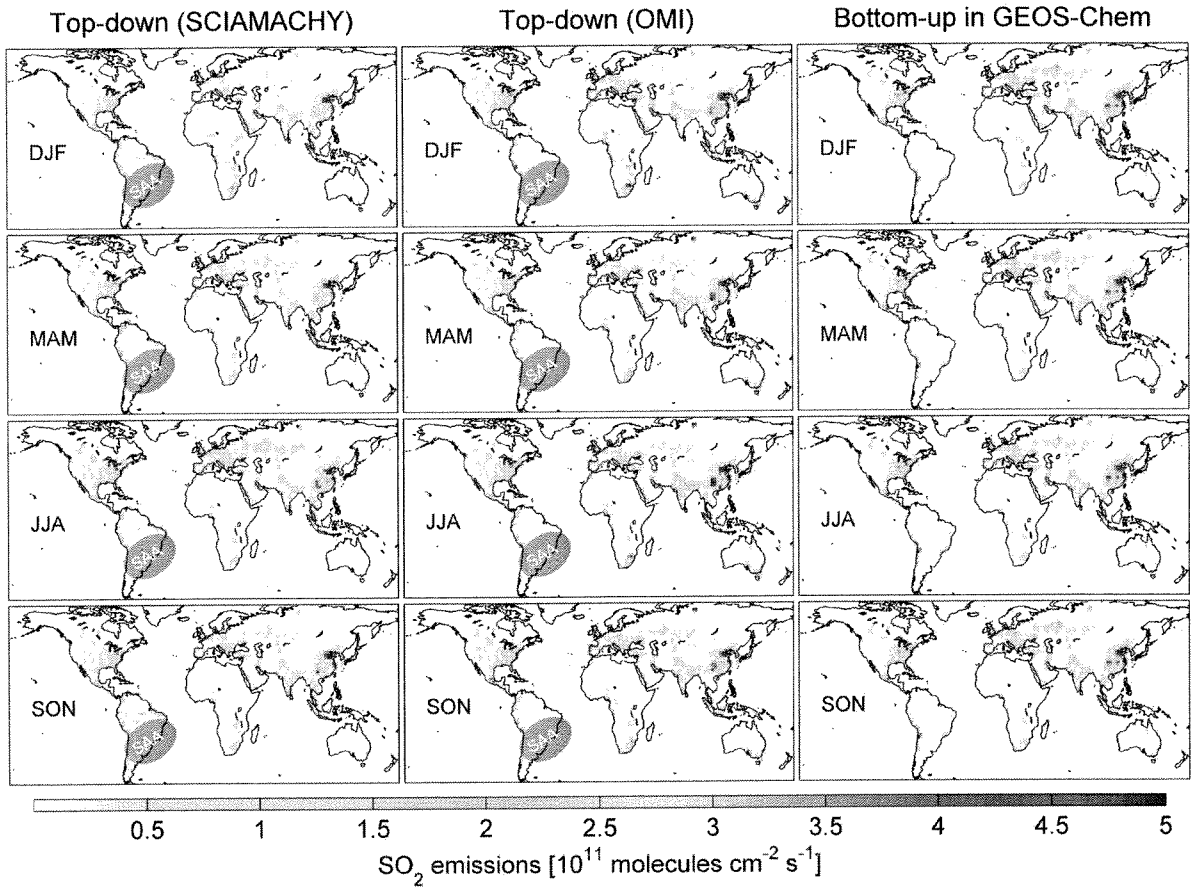

Figure 5. Seasonal mean anthropogenic SO_2 emissions from land with 2° × 2.5° horizontal resolution for the year 2006: (left) top-down emissions from SCIAMACHY, (middle) top-down emissions from OMI, and (right) bottom-up emissions in the GEOS-Chem model.

2007]. Land surface sources here include contributions from fossil fuels including coastal ships, biomass burning, biofuel burning, and continuously active volcanoes; it excludes contributions from ships in the open ocean, aircraft, or eruptive volcanoes. The mass balance approach is separately applied here to both SCIAMACHY and OMI. A better understanding of the differences between SCIAMACHY and OMI SO_2 columns is needed before exploiting diurnal variation in the inversion.

[37] Figure 5 presents the spatial and seasonal variation of top-down SO_2 emissions derived from SCIAMACHY and OMI, and the bottom-up SO_2 emissions in GEOS-Chem. Global annual anthropogenic SO_2 emissions over land and coastal ocean are 52.4 Tg S yr^{-1} from SCIAMACHY, 49.9 Tg S yr^{-1} from OMI, and 54.6 Tg S yr^{-1} from the bottom-up inventories. In support of the mass balance approach used here, there is little evidence in winter of greater smearing which would appear as reduced SO_2 emissions over sources, and enhanced SO_2 emissions downwind. The bottom-up emissions inventory exhibits little seasonal variation over major industrial regions [e.g., *Morris et al.*, 2007; *Zhang et al.*, 2009]. The weak seasonal variation in the top-down emissions (<15%) from both SCIAMACHY and OMI over major industrial regions provide confidence in the top-down approach. An exception is the Noril'sk smelter in Siberia (62.33°N, 88.22°E) where top-down emissions have a large seasonal component. Possible explanations are errors in the seasonal variation of simulated SO_2 oxidation, of retrieved SO_2 columns, or in the mass balance approach due to neglect of smearing. The global distribution of both top-down emissions are generally consistent (r = 0.78 for SCIAMACHY and 0.77 for OMI) with the bottom-up emissions. Higher correlations exist for the United States (r = 0.96 for SCIAMACHY and r = 0.94 for OMI) and China (r = 0.90 for SCIAMACHY and r = 0.93 for OMI). However, there are some significant regional differences discussed in the following paragraphs.

[38] Figure 6 evaluates the top-down inventories by intercomparing them. The top-down SO_2 emissions inferred from SCIAMACHY measurements are highly correlated (r = 0.92) with those from OMI measurements. However, the SCIAMACHY emissions are 20% higher than those from OMI, and there are regional differences (e.g., over Australia) which cannot be reconciled with the different overpass times of SCIAMACHY and OMI and may indicate satellite retrieval biases.

[39] Figure 7 shows the differences between the annual top-down and bottom-up emissions of SO_2. Here we

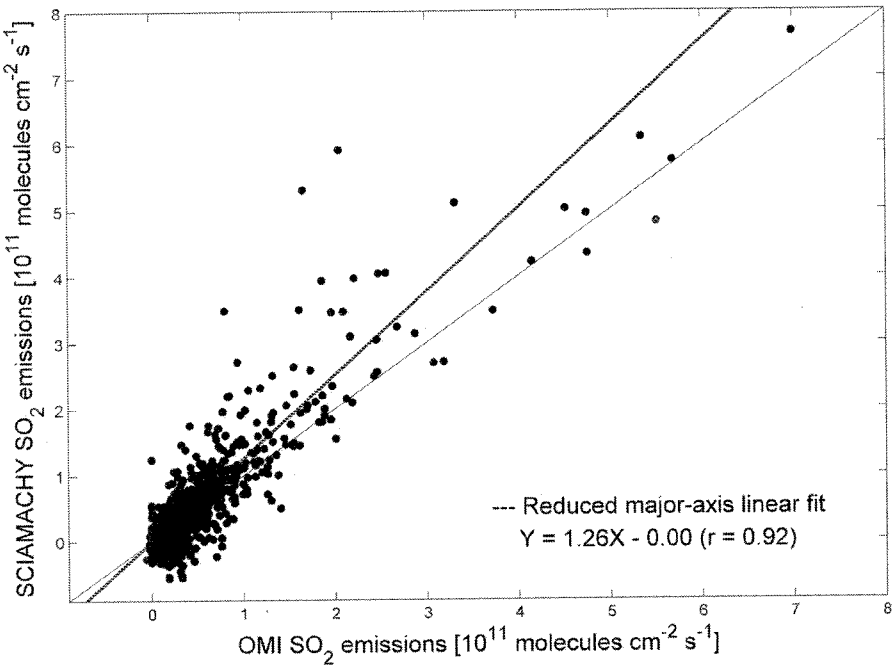

Figure 6. Scatterplot of the annual mean SO_2 emissions inferred from SCIAMACHY and OMI retrievals. The solid line represents the Y = X line, and the dotted line was calculated with the reduced major-axis linear regression [*Hirsch and Gilroy*, 1984].

exclude winter observations (SZA > 50°) which have higher uncertainty, and focus on regions where both SCIAMACHY and OMI have consistent results. Both top-down emissions are 10% lower over the eastern United States, within the uncertainty in the inversion and in the retrievals. The top-down emissions in China are lower by 50% for SCIAMACHY and 30% for OMI, except for near Beijing where they are higher by 30%. The bias over Nigeria may reflect effects of volcanic emissions in 2006. Several regions, such as the Highveld Plateau of South Africa, Mexico City, and northern India, have local differences of a factor of 2 that warrant further investigation.

6. Conclusion

[40] We produced a global top-down inventory of SO_2 emissions from satellite (SCIAMACHY and OMI) observations of SO_2 columns, through inverse modeling with a global chemical transport model (GEOS-Chem).

[41] We first evaluated the GEOS-Chem simulation of the SO_2 lifetime. The modeled SO_2 lifetime of 13 h for summer 2006 over the eastern United States is within 6 h (and within the 95% confidence level) of the in situ measurement-based SO_2 lifetime inferred from aircraft measurements for June to August, 1995–2005. We used the seasonal variation in the measured SO_2 mixing ratio over the eastern United States to estimate the seasonal variation in the SO_2 lifetime. The seasonal variation of the SO_2 lifetime inferred over the eastern United States from in situ measurements and from the GEOS-Chem simulation both indicate the SO_2 lifetime in winter is about three times as long as in summer. Thus the seasonal variation in SO_2 columns at northern midlatitudes is primarily driven by seasonal variation in the SO_2 loss rate, since SO_2 emissions exhibit little seasonal variation.

[42] We evaluated the SO_2 columns from the SCIAMACHY and OMI satellite instruments with surface SO_2 measurements. The surface SO_2 mixing ratios were derived from SCIAMACHY and OMI observations of SO_2 columns by applying coincident GEOS-Chem SO_2 profiles as a transfer function. The annual mean surface SO_2 concentrations from SCIAMACHY and OMI for 2006 exhibit a significant spatial correlation (r = 0.86, slope = 0.91 for SCIAMACHY and r = 0.81, slope = 0.79 for OMI) with the coincident in situ measurements throughout the United States and Canada from the U.S. EPA Air Quality System (AQS) and Environment Canada's National Air Pollution Surveillance (NAPS) networks.

[43] Sensitivity simulations reveal anthropogenic SO_2 emissions are dominant in the SO_2 column over most land areas. We used SO_2 columns from SCIAMACHY and OMI to derive seasonal top-down constraints for anthropogenic SO_2 emissions over land through inversion using the GEOS-Chem model. Global annual anthropogenic SO_2 emissions are 52.4 Tg S yr^{-1} from SCIAMACHY, 49.9 Tg S yr^{-1} from OMI, which are compared with the bottom-up emissions in the GEOS-Chem (54.6 Tg S yr^{-1}).

[44] The global distribution of the annual top-down emissions is spatially consistent with the bottom-up emissions (r = 0.78 for SCIAMACHY and 0.77 for OMI). The lack of seasonal variation in the top-down emissions (<10%) from both SCIAMACHY and OMI over most industrial regions provides some confidence in the top-down inventory. For the continental United States whose emission inventories are considered well-determined, top-down

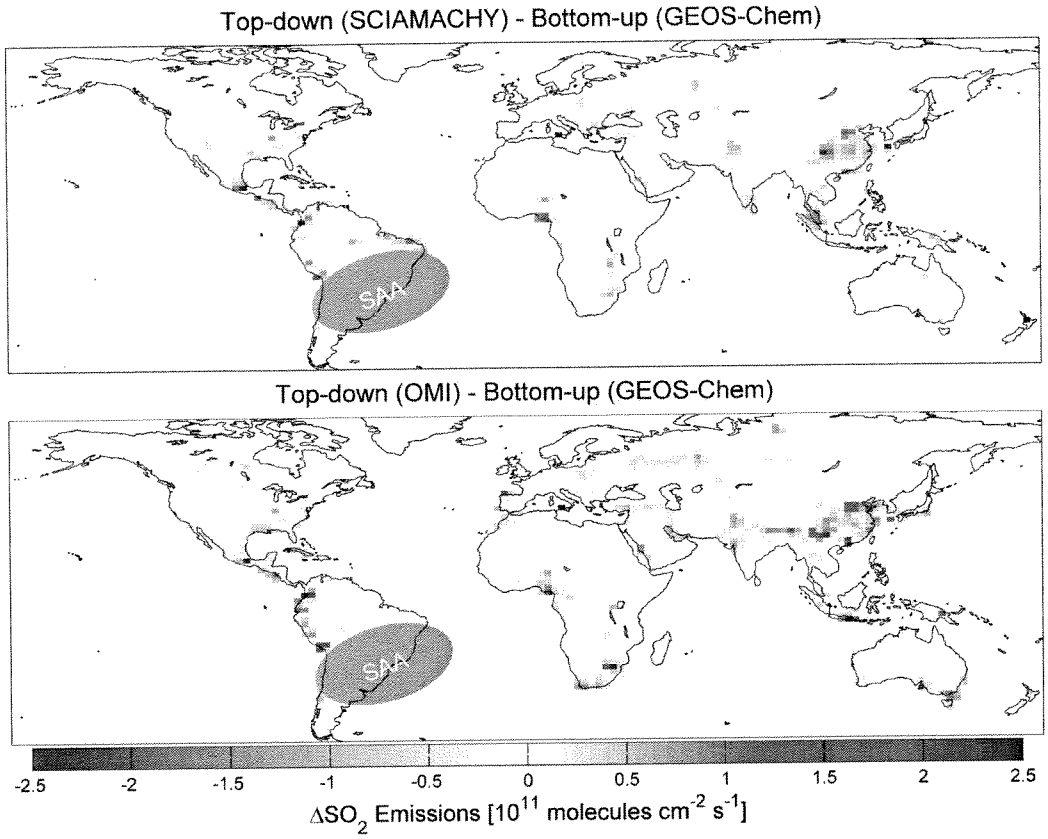

Figure 7. Difference between annual (top) SCIAMACHY and (bottom) OMI top-down and bottom-up emissions for the year 2006. Observations at solar zenith angles >50° are excluded.

emissions are highly consistent with bottom-up emissions (r = 0.96 for SCIAMACHY and r = 0.94 for OMI), with an overall bias of <20%. Top-down emissions for China which has higher SO_2 emissions are also highly spatially correlated (r = 0.90 for SCIAMACHY and r = 0.93 for OMI) with bottom-up emissions, but they are lower by 50% for SCIAMACHY and 30% for OMI, except for near Beijing where they are higher by 30%.

[45] This study could benefit from future work in several areas. Differences between SCIAMACHY and OMI SO_2 columns need to be reconciled. An a posteriori estimate that combines bottom-up and top-down emissions, weighted by their uncertainties, would better represent the true emission distribution. Inversion at higher spatial resolution should better account for spatial variance in the SO_2 lifetime. A more sophisticated inversion could improve its accuracy, could better account for smearing, and could enable extension to open ocean. A better understanding of SO_2 loss processes in winter is needed.

[46] **Acknowledgments.** We thank three anonymous reviewers for helpful comments. The publicly released Planetary Boundary Layer (PBL) OMI SO_2 Level 2 VC products were obtained from GES Data and Information Service Center (http://disc.sci.gsfc.nasa.gov/). SO_2 slant columns from SCIAMACHY were obtained from the Institute of Environmental Physics and Remote Sensing, University of Bremen, Germany (http://www.iup.uni-bremen.de/). This work was supported by Health Canada and by the National Aeronautics and Space Administration (NASA). Aircraft observations were supported by the Maryland Department of the Environment.

References

Afe, O. T., A. Richter, B. Sierk, F. Wittrock, and J. P. Burrows (2004), BrO emission from volcanoes: A survey using GOME and SCIAMACHY measurements, *Geophys. Res. Lett.*, *31*, L24113, doi:10.1029/2004GL020994.

Alexander, B., J. Savarino, C. C. W. Lee, R. J. Park, D. J. Jacob, M. H. Thiemens, Q. B. Li, and R. M. Yantosca (2005), Sulfate formation in sea-salt aerosols: Constraints from oxygen isotopes, *J. Geophys. Res.*, *110*, D10307, doi:10.1029/2004JD005659.

Alexander, B., R. J. Park, D. J. Jacob, and S. Gong (2009), Transition metal-catalyzed oxidation of atmospheric sulfur: Global implications for the sulfur budget, *J. Geophys. Res.*, *114*, D02309, doi:10.1029/2008JD010486.

Andres, R. J., and A. D. Kasgnoc (1998), A time-averaged inventory of subaerial volcanic sulfur emissions, *J. Geophys. Res.*, *103*(D19), 25,251–25,261, doi:10.1029/98JD02091.

Arellano, A. F., P. S. Kasibhatla, L. Giglio, G. R. van der Werf, and J. T. Randerson (2004), Top-down estimates of global CO sources using MOPITT measurements, *Geophys. Res. Lett.*, *31*, L01104, doi:10.1029/2003GL018609.

Berglen, T. F., T. K. Berntsen, S. A. Isaksen, and J. K. Sundet (2004), A global model of the coupled sulfur/oxidant chemistry in the troposphere: The sulfur cycle, *J. Geophys. Res.*, *109*, D19310, doi:10.1029/2003JD003948.

Bey, I., D. J. Jacob, R. M. Yantosca, J. A. Logan, B. D. Field, A. M. Fiore, Q. Li, H. Y. Liu, L. J. Mickley, and M. G. Schultz (2001), Global modeling of tropospheric chemistry with assimilated meteorology: Model description and evaluation, *J. Geophys. Res.*, *106*(D19), 23,073–23,095, doi:10.1029/2001JD000807.

Bhartia, P. K., and C. W. Wellemeyer (2002), TOMS-V8 total O_3 algorithm, *Algorithm Theoretical Basis Document, OMI Ozone Products, ATBD-OMI-02*, version 2.0, vol. II, edited by P. K. Bhartia, NASA Goddard Space Flight Cent., Greenbelt, Md. (available at http://eospso.gsfc.nasa.gov/eos_homepage/for_scientists/atbd/docs/OMI/ATBD-OMI-02.pdf)

Bogumil, K., et al. (2003), Measurements of molecular absorption spectra with the SCIAMACHY pre-flight Model: Instrument characterization and reference data for atmospheric remote sensing in the 230–2380 nm region, *J. Photochem. Photobiol. A*, *157*, 167–184, doi:10.1016/S1010-6030(03)00062-5.

Bovensmann, H., J. P. Burrows, M. Buchwitz, J. Frerick, S. Noel, V. V. Rozanov, K. V. Chance, and A. H. P. Goede (1999), SCIAMACHY: Mission objectives and measurement modes, *J. Atmos. Sci.*, *56*, 127–150, doi:10.1175/1520-0469(1999)056<0127:SMOAMM>2.0.CO;2.

Carn, S. A., L. L. Strow, S. de Souza-Machado, Y. Edmonds, and S. Hannon (2005), Quantifying tropospheric volcanic emissions with AIRS: The 2002 eruption of Mt. Etna (Italy), *Geophys. Res. Lett.*, *32*, L02301, doi:10.1029/2004GL021034.

Carn, S. A., A. J. Krueger, N. A. Krotkov, K. Yang, and P. F. Levelt (2007), Sulfur dioxide emissions Peruvian copper smelters detected by the Ozone Monitoring Instrument, *Geophys. Res. Lett.*, *34*, L09801, doi:10.1029/2006GL029020.

Chin, M., and D. J. Jacob (1996), Anthropogenic and natural contributions to tropospheric sulfate: A global model analysis, *J. Geophys. Res.*, *101*(D13), 18,691–18,699, doi:10.1029/96JD01222.

Chin, M., D. J. Jacob, G. M. Gardner, M. S. Foreman-Fowler, P. A. Spiro, and D. L. Savoie (1996), A global three-dimensional model of tropospheric sulfate, *J. Geophys. Res.*, *101*(D13), 18,667–18,690, doi:10.1029/96JD01221.

Eisinger, M., and J. P. Burrows (1998), Tropospheric sulfur dioxide observed by the ERS-2 GOME instrument, *Geophys. Res. Lett.*, *25*(22), 4177–4180, doi:10.1029/1998GL900128.

Evans, M. J., and D. J. Jacob (2005), Impact of new laboratory studies of N_2O_5 hydrolysis on global model budgets of tropospheric nitrogen oxides, ozone, and OH, *Geophys. Res. Lett.*, *32*, L09813, doi:10.1029/2005GL022469.

Fairlie, T. D., D. J. Jacob, and R. J. Park (2007), The impact of transpacific transport of mineral dust in the United States, *Atmos. Environ.*, *41*, 1251–1266, doi:10.1016/j.atmosenv.2006.09.048.

Fu, T.-M., D. J. Jacob, P. I. Palmer, K. Chance, Y. X. Wang, B. Barletta, D. R. Blake, J. C. Stanton, and M. J. Pilling (2007), Space-based formaldehyde measurements as constraints on volatile organic compound emissions in east and south Asia and implications for ozone, *J. Geophys. Res.*, *112*, D06312, doi:10.1029/2006JD007853.

Georgoulias, A. K., D. Balis, M. E. Koukouli, C. Meleti, A. Bais, and C. Zerefos (2009), A study of the total atmospheric sulfur dioxide load using ground-based measurements and the satellite derived sulfur dioxide Index, *Atmos. Environ.*, *43*, 1693–1701, doi:10.1016/j.atmosenv.2008.12.012.

Hains, J. C. (2007), A chemical climatology of lower tropospheric trace gases and aerosols over the mid-Atlantic region, Ph.D. diss., Univ. of Md., College Park.

Hains, J. C., B. F. Tabumann, A. M. Thompson, J. W. Stehr, L. T. Marufu, B. G. Doddridge, and R. R. Dickerson (2008), Origins of chemical pollution derived from mid-Atlantic aircraft profiles using a clustering technique, *Atmos. Environ.*, *42*, 1727–1741, doi:10.1016/j.atmosenv.2007.11.052.

Heald, C. L., D. J. Jacob, D. B. A. Jones, P. I. Palmer, J. A. Logan, D. G. Streets, G. W. Sachse, J. C. Gille, R. N. Hoffman, and T. Nehrkorn (2004), Comparative inverse analysis of satellite (MOPITT) and aircraft (TRACE-P) observations to estimate Asian sources of carbon monoxide, *J. Geophys. Res.*, *109*, D23306, doi:10.1029/2004JD005185.

Heald, C. L., D. J. Jacob, R. J. Park, B. Alexander, T. D. Fairlie, R. M. Yantosca, and D. A. Chu (2006), Transpacific transport of Asian anthropogenic aerosols and its impact on surface air quality in the United States, *J. Geophys. Res.*, *111*, D14310, doi:10.1029/2005JD006847.

Henze, D. K., A. Hakami, and J. H. Seinfeld (2007), Development of the adjoint of GEOS-Chem, *Atmos. Chem. Phys.*, *7*, 2413–2433, doi:10.5194/acp-7-2413-2007.

Hicks, B. B. (2006), Dry deposition to forests on the use of data from clearing, *Agric. Meteorol.*, *136*, 214–221, doi:10.1016/j.agrformet.2004.06.013.

Hirsch, R. M., and E. J. Gilroy (1984), Methods of fitting a straight line to data: Examples in water resources, *Water Resour. Bull.*, *20*(5), 705–711.

Intergovernmental Panel on Climate Change (2007), *Climate Change 2007: The Physical Science Basis, Contribution of Working Group I to the Fourth Assessment, Report of the Intergovernmental Panel on Climate Change*, edited by S. Solomon et al., Cambridge Univ. Press, Cambridge, U. K.

Jacob, D. J. (2000), Heterogeneous chemistry and tropospheric ozone, *Atmos. Environ.*, *34*, 2131–2159, doi:10.1016/S1352-2310(99)00462-8.

Jaeglé, L., R. V. Martin, K. Chance, L. Steinberger, T. P. Kurosu, D. J. Jacob, A. I. Modi, V. Yoboué, L. Sigha-Nkamdjou, and C. Gay-Lacaux (2004), Satellite mapping of rain-induced nitric oxide emissions from soils, *J. Geophys. Res.*, *109*, D21310, doi:10.1029/2004JD004787.

Katsouyanni, K., et al. (1997), Short term effects of ambient sulphur dioxide and particulate matter on mortality in 12 European cities: Results from time series data from the APHEA project, *BMJ Clin. Res. J.*, *314*, 1658–1663.

Khokhar, M. F., C. Frankenberg, M. Van Roozendael, S. Beirle, S. Kühl, A. Richter, U. Platt, and T. Wagner (2005), Satellite observation of atmospheric SO_2 from volcanic eruptions during the time-period of 1996–2002, *Adv. Space Res.*, *36*, 879–887, doi:10.1016/j.asr.2005.04.114.

Kopacz, M., D. J. Jacob, D. K. Henze, C. L. Heald, D. G. Streets, and Q. Zhang (2009), Comparison of adjoint and analytical Bayesian inversion methods for constraining Asian sources of carbon monoxide using satellite (MOPITT) measurements of CO columns, *J. Geophys. Res.*, *114*, D04305, doi:10.1029/2007JD009264.

Krotkov, N. A., S. A. Carn, A. J. Krueger, P. K. Bhartia, and K. Yang (2006), Band residual difference algorithm for retrieval of SO_2 from the Aura Ozone Monitoring Instrument (OMI), *IEEE Trans. Geosci. Remote Sens.*, *44*(5), 1259–1266, doi:10.1109/TGRS.2005.861932.

Krotkov, N. A., et al. (2008), Validation of SO_2 retrievals from the Ozone Monitoring Instrument (OMI) over NE China, *J. Geophys. Res.*, *113*, D16S40, doi:10.1029/2007JD008818.

Kuhns, H., E. M. Knipping, and J. M. Vukovich (2005), Development of a United States-Mexico emissions inventory for the Big Bend Regional Aerosol and Visibility Observational (BRAVO) study, *J. Air Waste Manage. Assoc.*, *55*, 677–692.

Lamsal, L. N., R. V. Martin, A. van Donkelaar, M. Steinbacher, E. A. Celarier, E. Bucsela, E. J. Dunlea, and J. P. Pinto (2008), Ground-level nitrogen dioxide concentrations inferred from the satellite-borne Ozone Monitoring Instrument, *J. Geophys. Res.*, *113*, D16308, doi:10.1029/2007JD009235.

Leaderer, B. P., T. R. Holford, and J. A. J. Stolwijk (1979), Relationship between sulfate aerosol and visibility, *J. Air Pollut. Control Assoc.*, *29*, 154–157.

Lee, C., A. Richter, M. Weber, and J. P. Burrows (2008), SO_2 retrieval from SCIAMACHY using the Weighting Function DOAS (WFDOAS) technique: Comparison with standard DOAS retrieval, *Atmos. Chem. Phys.*, *8*, 6137–6145, doi:10.5194/acp-8-6137-2008.

Lee, C., R. V. Martin, A. van Donkelaar, G. O'Byrne, N. Krotkov, A. Richter, L. G. Huey, and J. S. Holloway (2009), Retrieval of vertical columns of sulfur dioxide from SCIAMACHY and OMI: Air mass factor algorithm development, validation, and error analysis, *J. Geophys. Res.*, *114*, D22303, doi:10.1029/2009JD012123.

Leue, C., M. Wenig, T. Wagner, O. Klimm, U. Platt, and B. Jähne (2001), Quantitative analysis of NOx emissions from Global Ozone Monitoring Experiment satellite image sequences, *J. Geophys. Res.*, *106*, 5493–5505.

Levelt, P. F., G. H. J. van den Oord, M. R. Dobber, A. Malkki, H. Visser, J. de Vries, P. Stammes, J. O. V. Lundell, and H. Saari (2006), The Ozone Monitoring Instrument, *IEEE Trans. Geosci. Remote Sens.*, *44*, 1093–1101, doi:10.1109/TGRS.2006.872333.

Li, C., Q. Zhang, N. A. Krotkov, D. G. Streets, K. He, S.-C. Tsay, and J. F. Gleason (2010), Recent large reduction in sulfur dioxide emissions from Chinese power plants observed by the Ozone Monitoring Instrument, *Geophys. Res. Lett.*, *37*, L08807, doi:10.1029/2010GL042594.

Liu, Y., R. J. Park, D. J. Jacob, Q. Li, V. Kilaru, and J. A. Sarnat (2004), Mapping annual mean ground-level PM concentrations using Multiangle Imaging Spectroradiometer aerosol optical thickness over the contiguous United States, *J. Geophys. Res.*, *109*, D22206, doi:10.1029/2004JD005025.

Martin, R. V., D. J. Jacob, K. Chance, T. P. Kurosu, P. I. Palmer, and M. J. Evans (2003a), Global inventory of nitrogen oxide emissions constrained by space-based observations of NO_2 columns, *J. Geophys. Res.*, *108*(D17), 4537, doi:10.1029/2003JD003453.

Martin, R. V., D. J. Jacob, R. M. Yantosca, M. Chin, and P. Ginoux (2003b), Global and regional decreases in tropospheric oxidants from photochemical effects of aerosols, *J. Geophys. Res.*, *108*(D3), 4097, doi:10.1029/2002JD002622.

Millet, D. B., D. J. Jacob, K. F. Boersma, T.-M. Fu, T. P. Kurosu, K. Chance, C. L. Heald, and A. Guenther (2008), Spatial distribution of isoprene emissions from North America derived from formaldehyde column measurements by the OMI satellite sensor, *J. Geophys. Res.*, *113*, D02307, doi:10.1029/2007JD008950.

Morris, R. E., B. Koo, B. Wang, G. Stella, D. McNally, C. Loomis, C. J. Chien, and G. Tonnesen (2007), Technical support document for

VISTAS emissions and air quality modeling to support regional haze State Implementation Plans, technical report, VISTAS Tech. Coord. (Available at http://pah.cert.ucr.edu/vistas/docs.shtml)

Müller, J., and T. Stavrakou (2005), Inversion of CO and NO_2 emissions using the adjoint of the IMAGES model, *Atmos. Chem. Phys.*, *5*, 1157–1186, doi:10.5194/acp-5-1157-2005.

Myles, L., T. P. Meyers, and L. Robinson (2007), Relaxed eddy accumulation measurements of ammonia, nitric acid, sulfur dioxide and particulate sulfate dry deposition near Tampa, FL, USA, *Environ. Res. Lett.*, *2*, doi:10.1088/1748-9326/2/3/034004.

Olivier, J. G. J., J. J. M. Berdowski, J. A. H. W. Peters, J. Bakker, A. J. H. Visschedijk, and J. P. J. Bloos (2001), *Applications of EDGAR Including a Description of EDGAR 3.2: Reference Database with Trend Data for 1970–1995, RIVM Rep. 773301 001/NRP Rep. 410200 051*, RIVM, Bilthoven, Netherlands.

Palmer, P. I., D. J. Jacob, A. M. Fiore, and R. V. Martin (2003), Mapping isoprene emissions over North America using formaldehyde column observations from space, *J. Geophys. Res.*, *108*(D6), 4180, doi:10.1029/2002JD002153.

Park, R. J., D. J. Jacob, M. Chin, and R. V. Martin (2003), Sources of carbonaceous aerosols over the United States and implications for natural visibility, *J. Geophys. Res.*, *108*(D12), 4355, doi:10.1029/2002JD003190.

Park, R. J., D. J. Jacob, B. D. Field, and R. M. Yantosca (2004), Natural and transboundary pollution influences on sulphate-nitrate ammonium aerosols in the United States: Implications for policy, *J. Geophys. Res.*, *109*, D15204, doi:10.1029/2003JD004473.

Pétron, G., C. Granier, B. Khattatov, V. Yudin, J. F. Lamarque, L. Emmons, J. Gille, and D. P. Edwards (2004), Monthly CO surface sources inventory based on the 2000–2001 MOPITT satellite data, *Geophys. Res. Lett.*, *31*, L21107, doi:10.1029/2004GL020560.

Restad, K., I. S. A. Isaksen, and T. K. Berntsen (1998), Global distribution of sulfate in the troposphere: A three-dimensional model study, *Atmos. Environ.*, *32*, 3593–3609, doi:10.1016/S1352-2310(98)00081-8.

Richter, A., F. Wittrock, and J. P. Burrows (2006), SO_2 Measurements with SCIAMACHY, in *Proceeding of Atmospheric Science Conference, Frascati, Italy, 8–12 May, ESA Publ. SP-628*, ESA/ESRIN, Noordwijk, Netherlands.

Schakenbach, J., R. Vollaro, and R. Forte (2006), Fundamentals of successful monitoring, reporting, and verification under a cap-and-trade program, *J. Air Waste Manage. Assoc.*, *56*, 1576–1583.

Schwab, J. J., J. B. Spicer, and K. L. Demerjian (2009), Ozone, trace gas, and particulate matter measurements at a rural site in southwestern New York state: 1995–2005, *J. Air Waste Manage. Assoc.*, *59*, 293–309, doi:10.3155/1047-3289.59.3.293.

Smith, S. J., J. van Aardenne, Z. Klimont, R. Andres, A. Volke, and S. Delgado Arias (2010), Anthropogenic sulfur dioxide emissions: 1850–2005, *Atmos. Chem. Phys. Discuss.*, *10*, 16,111–16,151, doi:10.5194/acpd-10-16111-2010.

Spinei, E., S. A. Carn, N. A. Krotkov, G. H. Mount, K. Yang, and A. J. Krueger (2010), Validation of OMI SO_2 measurements in the Okmok volcanic cloud over Pullman, WA, July 2008, *J. Geophys. Res.*, D00L08, doi:10.1029/2009JD013492.

Spurr, R. J. D. (2002), Simultaneous derivation of intensities and weighting functions in a general pseudo-spherical discrete ordinate radiative transfer treatment, *J. Quant. Spectrosc. Radiat. Transf.*, *75*, 129–175, doi:10.1016/S0022-4073(01)00245-X.

Spurr, R. J. D., T. P. Kurosu, and K. V. Chance (2001), A linearized discrete ordinate radiative transfer model for atmospheric remote-sensing retrieval, *J. Quant. Spectrosc. Radiat. Transf.*, *68*, 689–735, doi:10.1016/S0022-4073(00)00055-8.

Taubman, B. F., J. C. Hains, A. M. Thompson, L. T. Marufu, B. G. Doddridge, J. W. Stehr, C. A. Piety, and R. R. Dickerson (2006), Aircraft vertical profiles of trace gas and aerosol pollution over the mid-Atlantic United States: Statistics and meteorological cluster analysis, *J. Geophys. Res.*, *111*, D10S07, doi:10.1029/2005JD006196.

Thomas, W., T. Erbertseder, T. Ruppert, M. Van Roozendael, J. Verdebout, D. Balis, C. Meleti, and C. Zerefos (2005), On the retrieval of volcanic sulfur dioxide emissions from GOME backscatter measurements, *J. Atmos. Chem.*, *50*, 295–320, doi:10.1007/s10874-005-5544-1.

U.S. Climate Change Science Program (2009), *Atmospheric aerosol properties and climate impacts, A Report by the U.S. Climate Change Science Program and the Subcommittee on Global Change Research*, edited by M. Chin, R. Kahn, and S. E. Schwartz, Natl. Aeronaut. and Space Admin., Washington, D. C.

U.S. Environmental Protection Agency (2009), *National Emissions Inventory (NEI) Air Pollutant Emissions Trends Data*, U.S. EPA, Washington, D. C. (Available at http://www.epa.gov/ttnchie1/trends/)

Vandaele, A. C., P. C. Simon, J. M. Guilmot, M. Carleer, and R. Colin (1994), SO_2 absorption cross section measurement in the UV using a Fourier transform spectrometer, *J. Geophys. Res.*, *99*, 25,599–25,605, doi:10.1029/94JD02187.

van Donkelaar, A., R. V. Martin, and R. J. Park (2006), Estimating ground-level PM2.5 using aerosol optical depth determined from satellite remote sensing, *J. Geophys. Res.*, *111*, D21201, doi:10.1029/2005JD006996.

van Donkelaar, A., et al. (2008), Analysis of aircraft and satellite measurements from the Intercontinental Chemical Transport Experiment (INTEX-B) to quantify long-range transport of East Asian sulfur to Canada, *Atmos. Chem. Phys.*, *8*, 2999–3014, doi:10.5194/acp-8-2999-2008.

van Donkelaar, A., R. V. Martin, M. Brauer, R. Kahn, R. Levy, C. Verduzco, and P. J. Villeneuve (2010), Global estimates of exposure to fine particulate matter concentrations from satellite-based aerosol optical depth: Development and application, *Environ. Health Perspect.*, *118* (6), 847–855, doi:10.1289/ehp.0901623.

Vountas, M., V. V. Rozanov, and J. P. Burrows (1998), Ring effect: Impact of rotational Raman scattering on radiative transfer in Earth's atmosphere, *J. Quant. Spectrosc. Radiat. Transf.*, *60*, 943–961, doi:10.1016/S0022-4073(97)00186-6.

Wang, C., J. J. Corbett, and J. Firestone (2008), Improving spatial representation of global ship emissions inventories, *Environ. Sci. Technol.*, *42*, 193–199, doi:10.1021/es0700799.

Yang, K., N. A. Krotkov, A. J. Krueger, S. A. Carn, P. K. Bhartia, and P. F. Levelt (2007), Retrieval of large volcanic SO_2 columns from the Aura Ozone Monitoring Instrument: Comparison and limitations, *J. Geophys. Res.*, *112*, D24S43, doi:10.1029/2007JD008825.

Zhang, Q., et al. (2009), Asian emissions in 2006 for the NASA INTEX-B mission, *Atmos. Chem. Phys.*, *9*, 5131–5153, doi:10.5194/acp-9-5131-2009.

R. R. Dickerson and K. Vinnikov, Department of Atmospheric and Oceanic Science, University of Maryland, College Park, MD 20742, USA.

J. C. Hains, Maryland Department of the Environment, Baltimore, MD 21230, USA.

N. Krotkov, Goddard Earth Sciences and Technology Center, University of Maryland, Baltimore County, Baltimore, MD 21228, USA.

C. Lee, National Institute of Meteorological Research, Korea Meteorological Administration, 45 Gisangcheong-gil, Dongjak-gu, Seoul 156-720, South Korea.

H. Lee, Department of Atmospheric Science, Yonsei University, Seoul 120-749, South Korea.

R. V. Martin and A. van Donkelaar, Department of Physics and Atmospheric Science, Dalhousie University, Halifax, Nova Scotia B3H 3J5, Canada.

A. Richter, Institute of Environmental Physics and Remote Sensing, University of Bremen, Bremen D-28334, Germany.

J. J. Schwab, Atmospheric Sciences Research Center, University at Albany, State University of New York, NY 12203, USA.